Strong Field Theories beyond Dipole Approximations in Nonrelativistic Regimes

Pei-Lun He,* Di Lao,† and Feng He‡
Key Laboratory for Laser Plasmas (Ministry of Education) and School of Physics and Astronomy, Collaborative Innovation Center of IFSA (CICIFSA), Shanghai Jiao Tong University, Shanghai 200240, China
(Received 31 October 2016; revised manuscript received 9 February 2017; published 21 April 2017)

The exact nondipole Volkov solutions to the Schrödinger equation and Pauli equation are found, based on which a strong field theory beyond the dipole approximation is built for describing the nondipole effects in nonrelativistic laser driven electron dynamics. This theory is applied to investigate momentum partition laws for multiphoton and tunneling ionization and explicitly shows that the complex interplay of a laser field and Coulomb action may reverse the expected photoelectron momentum along the laser propagation direction. The magnetic-spin coupling does not bring observable effects on the photoelectron momentum distribution and can be neglected. Compared to the strong field approximation within the dipole approximation, this theory works in a much wider range of laser parameters and lays a solid foundation for describing nonrelativistic electron dynamics in both short wavelength and midinfrared regimes where nondipole effects are unavoidable.

DOI: 10.1103/PhysRevLett.118.163203

Two kinds of processes are very fundamental in ultrafast laser-atom and laser-molecule interactions, i.e., the deposition of photon energies into atoms and molecules and the transfer of photon linear momentum into targets. Plenty of studies focused on the energy deposition and a series of intriguing ultrafast phenomena were explored, such as tunneling ionization [1], high harmonic generation and its synthesization of attosecond light pulses [2], nonsequential double ionization [3], coherent control of electron localization [4–7], and energy sharing between electrons and nuclei [8]. For the second one, the transfer of photon linear momentum attracts much less attention due to the fact that a photon is not an effective momentum carrier as compared to a nonrelativistic electron.

Thanks to the detection techniques with high resolutions developed recently, Smeenk *et al.* [9] and Ludwig *et al.* [10] reported that photoelectrons acquire a momentum shift along the direction of laser propagation (termed as longitudinal momentum shift in the rest of the Letter) during tunneling ionization, and this photon momentum transfer is also reported in the time-dependent Dirac equation simulation [11], time-dependent Schrödinger equation (TDSE) simulations [12,13], and classical trajectory Monte Carlo calculations [14]. Some characters of the longitudinal momentum shift [15–20] were explored by calculations of strong field approximation (SFA). Though it is well recognized that the longitudinal momentum shift must be due to the nondipole laser-atom coupling, the exact nondipole Volkov solution was not built into these studies. To circumvent this obstacle, some attempts have been tried. Chelkowski *et al.* adopted the Volkov solution of the Klein-Gordon equation in their SFA calculations [19]. Krajewska *et al.* made an analogy with quantum electrodynamics in obtaining the transition amplitude [21]. Cricchio and others rewrote the space-time dependent laser vector potential as $\mathbf{A}(\mathbf{x},t)\approx\mathbf{A}(t)+(z/c)\mathbf{E}(t)$ [18,22–24]. Here, $\mathbf{A}(t)$ and $\mathbf{E}(t)$ are the dipole approximated laser vector potential and laser electric field, and c is the light speed. To build a self-consistent strong field theory beyond the dipole approximation is still difficult because there is no exact nondipole Volkov wave function to the Schrödinger equation until today, though the Volkov solution to the Schrödinger equation within the dipole approximation had been obtained around eighty years ago.

In this Letter, we analytically solved the TDSE for a free electron in a monochromatic laser field and achieved the exact nondipole Volkov solution. Based on this, we built the nondipole SFA theory, which is then applied to describing how the electron acquires the momentum along the laser propagation direction, and how rescattering alters the photon momentum partition between electrons and nuclei. For very wide ranges of laser parameters, this theory is self-consistent and is able to grasp the main dynamics and offer intuitive physical explanations with easy computations.

We used the light cone coordinate $\eta=t-(z/c)$ to describe the laser pulse by assuming it propagates along the z axis. The components of the laser vector potential are $\mathbf{A}(\mathbf{r},t)=\mathbf{A}(\eta)=(A_x(\eta),A_y(\eta),0)$. The behavior of a free electron embedded in such a laser field is described by the TDSE as [atomic units (a.u.) are used unless stated otherwise]

$$i\frac{\partial}{\partial t}\psi_V(\mathbf{r},t)=\frac{1}{2}\{[\mathbf{p}_\perp+\mathbf{A}_\perp(\eta)]^2+p_z^2\}\psi_V(\mathbf{r},t), \quad (1)$$

with $\mathbf{p}$ being the electron momentum operator. We conjectured that the Volkov solution of Eq. (1) has the form

$\psi_V(\mathbf{r},t)=\exp(-iE_\mathbf{p}t+i\mathbf{p}\cdot\mathbf{r})f(\eta)$ with $E_\mathbf{p}=\frac{1}{2}\mathbf{p}^2$ and $f(\eta)$ is temporarily unknown. Inserting the conjectured $\psi_V(\mathbf{r},t)$ into Eq. (1) yields the governed equation for $f(\eta)$

$$i\left(1-\frac{p_z}{c}\right)f'(\eta)=H_I(\eta)f(\eta)-\frac{1}{2c^2}f''(\eta), \tag{2}$$

with the interaction Hamiltonian $H_I(\eta)=\mathbf{A}(\eta)\cdot\mathbf{p}+\frac{1}{2}\mathbf{A}^2(\eta)$. The solution of Eq. (2) is $f(\eta)=G(\eta)f_0(\eta)$ with $f_0(\eta)=\exp(-i\int^\eta d\xi\{[\mathbf{A}(\xi)\cdot\mathbf{p}+(1/2)\mathbf{A}^2(\xi)]/(1-p_z/c)\})$ and $G(\eta)=T(\exp\{i\int^\eta d\xi[f_0^*(\xi)\frac{d^2}{d\xi^2}f_0(\xi)]/[2c^2(1-p_z/c)]\})$ with T being the ordering operator [25]. For any general function $F(\xi)$,

$$\begin{aligned}&T\left[\exp\left(i\int_{\xi_0}^{\eta}d\xi F(\xi)\right)\right]\\&=1+i\int_{\xi_0}^{\eta}d\xi_1F(\xi_1)\\&\quad+i^2\int_{\xi_0}^{\eta}d\xi_1F(\xi_1)\left(\int_{\xi_0}^{\xi_1}d\xi_2F(\xi_2)\right)+\cdots.\end{aligned} \tag{3}$$

In the above expressions, the differential operator acts on all the later terms, i.e., $F(\xi_1)[\int_{\xi_0}^{\xi_1}d\xi_2F(\xi_2)]\sim(d^2/d\xi_1^2)[f_0(\xi_1)\int_{\xi_0}^{\xi_1}d\xi_2F(\xi_2)]$. The exact Volkov solution beyond the dipole approximation is then achieved.

With the analytical expression of the nondipole Volkov state, one may write down the transition amplitude beyond the dipole approximation

$$\begin{aligned}W^{(1)}(\mathbf{p})=-i\int_{t_0}^{t_f}d\eta G^*(\eta)[\mathbf{A}(\eta)\cdot\mathbf{p}+\tfrac{1}{2}\mathbf{A}^2(\eta)]\\\times\exp[i(S_\mathbf{p}(\eta)+I_p\eta)]\tilde{\phi}_0\left(\mathbf{p}_\perp,p_z-\frac{E_\mathbf{p}+I_p}{c}\right),\end{aligned} \tag{4}$$

where $S_\mathbf{p}(\eta)=\int^\eta dt\{E_\mathbf{p}+[\mathbf{A}(t)\cdot\mathbf{p}+\frac{1}{2}\mathbf{A}^2(t)]/[(1-p_z/c)]\}$ is the Volkov phase, and $\tilde{\phi}_0(\mathbf{p})=\int d\mathbf{r}\exp(-i\mathbf{p}\cdot\mathbf{r})\phi_0(\mathbf{r})$. One may recognize that Eq. (4) changes into the dipole transition amplitude as $c\to+\infty$.

Since the Schrödinger equation is the nonrelativistic version of the Klein-Gordon equation, by truncating the terms at $\sim(1/c^2)$ when expanding $H=\sqrt{m^2c^4+\mathbf{p}^2c^2}=mc^2+(\mathbf{p}^2/2m)+O(1/c^2)$, only the correction up to $O(1/c)$ in our SFA theory should be anticipated after considering the nondipole effect, and the correction higher than the order of $O(1/c)$ is logically unnecessary. One may note that $f_0(\eta)$ is already corrected up to $O(1/c)$; thus, only the leading term on the right-hand side of Eq. (3) is important.

With the nondipole SFA, one may calculate the longitudinal momentum shift induced by the nondipole coupling. We treated the transition amplitude given by Eq. (4) in different forms, for example, replacing the term $[1/(1-p_z/c)]$ by $1+(p_z/c)$, or only keeping the leading term of Eq. (4), i.e., $G(\eta)\to1$. The numerically calculated expected values (denoted by $\langle\rangle$) of longitudinal momenta $\langle p_z\rangle$ are summarized in Table I. The used laser pulse is right-handed circularly polarized, and the intensity and wavelength are 10^{14} W/cm^2 and 1400 nm, and the initial state is the ground state of a hydrogen atom. These laser parameters are similar to those used in Refs. [9,19], and the law $\langle p_z\rangle\approx(\langle E_\mathbf{p}\rangle+0.3I_p)/c$ is reproduced, where $\langle E_\mathbf{p}\rangle$ is the expected kinetic energy of the photoelectron. The deviation of the exact result and approximated results is within the order of $\sim(1/c^2)$, which is consistent with our analysis. The simulation results confirm that taking the leading term in the Dyson expression of $G(\eta)$ will not bring any observable error with the current experimental detection resolution. Hence, in the later calculations, we simply set $G(\eta)=1$ in the nondipole Volkov state. More properties of $G(\eta)$ are presented in the Supplemental Material [26].

TABLE I. The expected value of longitudinal momenta $\langle p_z\rangle$ calculated with different schemes. In these calculations, a wavelength 1400 nm right-handed circularly polarized laser pulse with the intensity 10^{14} W/cm^2 is used and the target hydrogen atom is in the ground state.

Calculation Schemes	$\langle p_z\rangle$ (a.u.)
Dipole approximation	0
Exact calculation	6.8×10^{-3}
$G(\eta)\to1$	6.8×10^{-3}
$G(\eta)\to1$ and $[1/(1-p_z/c)]\to1+\frac{p_z}{c}$	6.8×10^{-3}
$G(\eta)\to1$ and $[1/(1-p_z/c)]\to1$	5.3×10^{-4}

Gauge invariance is not preserved in the nondipole SFA. In length gauge, with the same parameters used in Table I, we reached $\langle p_z\rangle\approx(\langle E_\mathbf{p}\rangle+\frac{1}{3}I_p)/c$ [18]. Though the velocity gauge is more intuitive for describing results, the length gauge is more quantitatively accurate in this research. Actually, the SFA in the velocity gauge gives identical photoelectron momentum distributions when the initial state has opposite magnetic quantum numbers and the laser pulse is circularly polarized, which contradicts the known facts [29,30]. Thus, all subsequent numerical calculations are carried out in length gauge in this Letter. With a unitary phase transformation $\exp[i\mathbf{A}(\eta)\cdot\mathbf{x}]$, the transition amplitude in the length gauge is obtained

$$\begin{aligned}W_L^{(1)}(\mathbf{p})=-i\int_{t_0}^{t_f}d\eta\exp[i(S_\mathbf{p}(\eta)+I_p\eta)]\left(1-\frac{p_z}{c}\right)\mathbf{E}(\eta)\\\cdot i\frac{\partial}{\partial\mathbf{k}}\tilde{\phi}_0(\mathbf{k})|_{\mathbf{k}=[\mathbf{p}_\perp+\mathbf{A}(\eta),p_z-(E_\mathbf{p}+I_p)/c]},\end{aligned} \tag{5}$$

where $\mathbf{E}(\eta)=-(\partial/\partial t)\mathbf{A}(\eta)$ is the electric field.

As one of the application examples, we used the nondipole SFA theory to investigate the photon momenta partition between nuclei and electrons. For an electron initially in the ground state of the hydrogen atom $(n,l,m)=(1,0,0)$, applying Eq. (4) with the plane wave laser for the single-photon ionization limit and the imaginary time method [31] in the tunneling ionization limit (where the electric field is treated as quasistatic and the magnetic field is treated via perturbations), we obtained the analytical formula

$$\langle p_z\rangle_s=\frac{8}{5}\frac{\langle E_{\mathbf{p}}\rangle}{c(1-\frac{U_p}{\omega})}-\frac{U_p}{c},\qquad \langle p_z\rangle_t=\frac{\langle E_{\mathbf{p}}\rangle+I_p}{c},\qquad (6)$$

where $U_p=[\int_0^{\mathrm{T}}dt\frac{1}{2}\mathbf{A}^2(t)/\mathrm{T}]$ is the ponderomotive energy, i.e., the averaged quiver kinetic energy, and T and ω are the optical period and frequency, respectively. The omission of U_p terms makes $\langle p_z\rangle_s=\frac{8}{5}(\langle E_{\mathbf{p}}\rangle/c)$ [19]. For the tunneling ionization, the first term of $\langle p_z\rangle_t$ originates from the classical electron electrodynamics in the continuum and the second term of $\langle p_z\rangle_t$ is contributed by the under-the-barrier dynamics [32]. $\langle p_z\rangle_t$ is affected by the detail of the under-the-barrier dynamics [19,32], where the laser intensity and electronic state play a role. More details on the formula derivations and discussions can be found in the Supplemental Material [26].

Between these two limiting cases, the expected longitudinal momentum shift can be formulated as

$$\langle p_z\rangle=\frac{\alpha\langle E_{\mathbf{p}}\rangle+\beta I_p+\gamma U_p}{c},\qquad (7)$$

where α, β, and γ are fitting parameters depending on the absorbed photon number N, which is determined by the floor function $N=\lfloor I_p/\omega\rfloor+1$. To calibrate the N-dependent α, β, and γ, we finely tuned the laser frequency ω within $[I_p/N, I_p/(N-1)]$, and fit $\langle p_z\rangle$ expressed by Eq. (7) to obtain α, β, and γ for a certain N. Figure 1 shows the fitted α, β, and γ. Here, the laser pulse is circularly polarized and its intensity is 10^{14} W/cm^2. The initial state is the ground state of the hydrogen atom. The fitted parameters $\alpha=1.6$, $\beta=0$ for $N=1$ are consistent with the analytical results. However, in such a situation, $\langle p_z\rangle\approx 4\times10^{-3}$ a.u., while $(U_p/c)\approx 4\times10^{-6}$ a.u. is numerically too small to extract γ accurately by the least squares fitting method adopted here. Thus, in Fig. 1(c), we fit γ for $N\geq 4$ where (U_p/c) is relatively large and the extracted γ is reliable. With the increasing of N, we observed the tendencies $\alpha\to 1$, $\gamma\to 0$, and $\beta\to\frac{1}{3}$. The asymptotic value of β agrees with that obtained in [32], where the short range potential was used.

To gain more insights into how the momentum is partitioned in the tunneling regime, in Fig. 2(a), we plotted $\langle p_z\rangle$ as a function of the laser intensity when the electron is initially in different states. The laser is right-handed circularly polarized and the wavelength is 1400 nm. The calculated intensity-dependent $\langle p_z\rangle$ shares a similar shape as that measured in Ref. [9]. When the intensity is larger than 3×10^{13} W/cm^2, α approaches 1 and γ approaches 0; however, the varying β results in the deviation of the linear relationship between $\langle p_z\rangle$ and the laser intensity. The β response can be more clearly seen in Fig. 2(b), where $\Delta p_z=\langle p_z\rangle-\langle E_{\mathbf{p}}\rangle/c$ is plotted. It is clear that $\beta\approx\frac{1}{3}$ only holds for the initial state $(n,l,m)=(1,0,0)$ in strong laser pulses. This could be due to the fact that the electronic state of $(n,l,m)=(1,0,0)$ is somehow close to the bound state

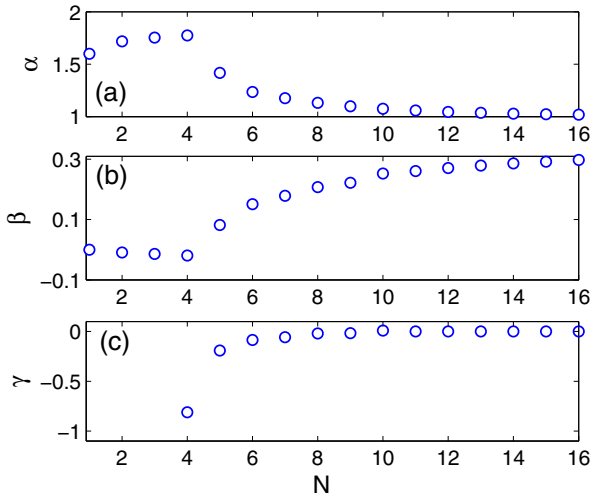

FIG. 1. (a) The fitted (a) α, (b)β, and (c) γ as a function of the absorbed photon number N. The laser intensity is fixed at 10^{14} W/cm^2, and the initial electronic state is the hydrogen ground state $(n,l,m)=(1,0,0)$.

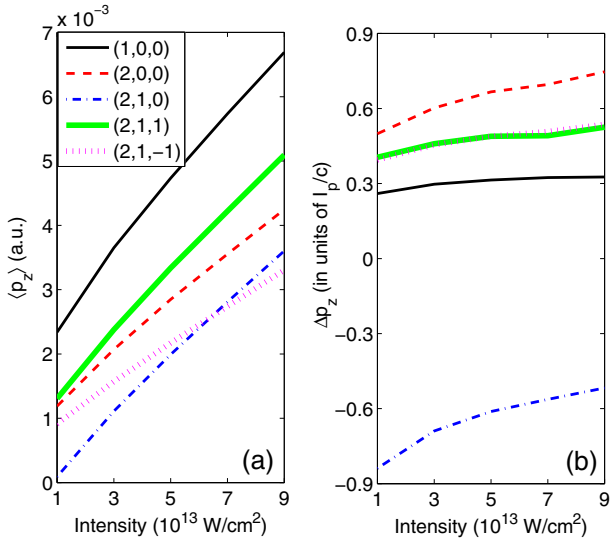

FIG. 2. (a)$\langle p_z\rangle$ and (b)Δp_z as a function of the laser intensity. The laser wavelength is 1400 nm and right-handed circularly polarized. (a) and (b) share the same graph legend.

of a short range potential. Our simulations also demonstrate that the photon-momentum partition closely relates to the initial angular momentum. It is also interesting to note that, while curves of (2,1,1) and $(2,1,-1)$ are different in Fig. 2(a), they are overlapped in Fig. 2(b). This conclusion also works for other $(n,l,\pm m)$ pairs.

The longitudinal momentum shift is more complicated if the driving laser pulse is linearly polarized since the rescattering occurs and the Coulomb potential plays an important role. Thus, we extended the nondipole SFA theory by including the Coulomb potential via the first-order Born approximation [33]. Similarly, the transition amplitude, after taking into account the Coulomb potential in the nondipole SFA, is written as

$$W^{(2)}(\mathbf{p}) = (-i)^2 \int_{t_0}^{t_f} d\tau' \int_{t_0}^{\tau'} d\tau \int \frac{\mathrm{d}^3 k}{(2\pi)^3} \times \langle \mathbf{p}_V(\tau')|V_c|\mathbf{k}_V(\tau')\rangle \langle \mathbf{k}_V(\tau)|H_I(\tau)|\phi_0(\tau)\rangle, \quad (8)$$

where $|\mathbf{k}_V\rangle$ is the intermediate nondipole Volkov state, and V_c is the Coulomb potential. After more arithmetic calculations, Eq. (8) changes into

$$W^{(2)}(\mathbf{p}) = (-i)^2 \int \frac{d^3k}{(2\pi)^3} \int_{t_0}^{t_f} dx_1 \int_{t_0}^{x_1} dx_2 H_I(x_2) \times \exp\{i[S_{\mathbf{p}}(x_1) - S_{\mathbf{k}}(x_1) + S_{\mathbf{k}}(x_2) + I_p x_2]\} \times \tilde{V}_c\left(\mathbf{p}_\perp - \mathbf{k}_\perp, p_z - k_z - \frac{E_{\mathbf{p}} - E_{\mathbf{k}}}{c}\right) \times \tilde{\phi}_0\left(\mathbf{k}_\perp, k_z - \frac{E_{\mathbf{k}} + I_p}{c}\right), \quad (9)$$

where $\tilde{V}_c \propto 1/[(\mathbf{p}-\mathbf{k})^2 + \sigma]$ is the Fourier transformation of $V_c = -(1/|\mathbf{r}|)\exp(-\sqrt{\sigma}|\mathbf{r}|)$ and σ is the screening parameter for the Coulomb potential. Equation (9) is identical to Eq. (8) in the sense that the contribution of a finite target size is negligible [26]. The integration over the intermediate nondipole Volkov state $|\mathbf{k}_V\rangle$ is carried out via the steepest descents method with the saddle points determined by $\nabla_{\mathbf{k}}[S_{\mathbf{k}}(x_1) - S_{\mathbf{k}}(x_2)] = 0$, which means the integral of Eq. (9) is dominated by events that electrons released at x_2 come back to the nuclei at x_1. The scaled momentum distribution $\int d\mathbf{p}_\perp |W^{(1)}(\mathbf{p}) + W^{(2)}(\mathbf{p})|^2$ are plotted in Fig. 3(a). The narrower momentum distribution for smaller σ is due to the stronger Coulomb focusing effect. Note that $W \approx W^{(1)} + W^{(2)}$ diverges for $\sigma < 1$ and converges for $\sigma \geq 1$, and thus, the curves for $\sigma = 0.1$ and 0.01 deviate from real physics. The divergency could possibly be cured by summing divergent terms into a unitary phase [34].

We plotted $\langle p_z \rangle$ as a function of the laser intensity by including both the direct and rescattering ionization events in Fig. 3(b). The laser field is linearly polarized and the wavelength is 3400 nm, as used in the experiment [10].

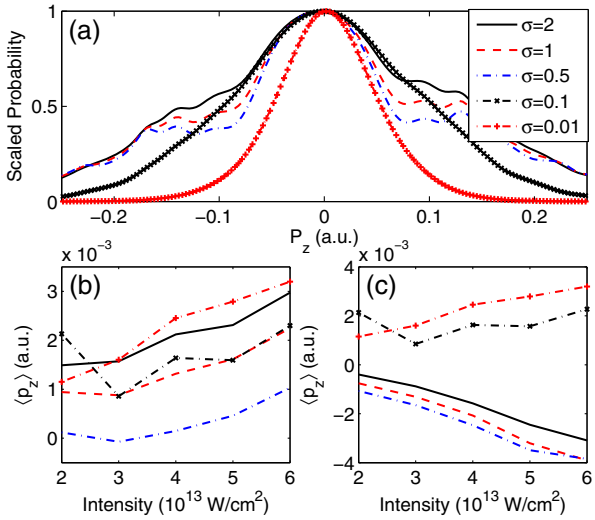

FIG. 3. (a) The scaled longitudinal momentum distribution when different screening parameters σ are used. (b) $\langle p_z \rangle$ as a function of the laser intensity, in which calculations, both the direct and rescattering ionization events are included. (c) $\langle p_z \rangle$ as a function of the laser intensity, where only rescattering events are taken into account. (a), (b), and (c) share the same graph legend.

Similar to Fig. 2(a), where the circularly polarized laser pulse is used, the overall shift of the expected longitudinal momentum increases with the increasing of the laser intensity. Note that Fig. 3(b) presents $\langle p_z \rangle$ while Ref. [10] presented the peak offset of the photoelectron longitudinal momentum distribution. The calculated peak shift of the photoelectron longitudinal momentum distribution as a function of the laser intensity is shown in the Supplemental Material [26]. Figure 3(c) shows $\langle p_z \rangle$ by only including the rescattering events. We reminded that the curves of $\sigma < 1$ do not express the physics correctly, while the converged results of $\sigma = 1$ or 2 clearly depict the negative shift of $\langle p_z \rangle$ induced by rescattering.

So far, the electronic spin dynamics is not touched. The spin-magnetic coupling is in the order of $O(1/c)$, the same as the leading order of the electric nondipole coupling. Thus, it is conceptually important to note that the break down of the dipole approximation at the nonrelativistic regime also implies the break down of the spin-0 approximation for electrons. To study the nondipole effect in photoionization more completely, we extended the Schrödinger equation to the Pauli equation by including the spin-magnetic coupling

$$i\frac{\partial}{\partial t}\phi(\mathbf{r},t) = \left(\frac{1}{2}[\mathbf{p} + \mathbf{A}(\eta)]^2 + \frac{\boldsymbol{\sigma}}{2}\cdot\mathbf{B}(\eta)\right)\phi(\mathbf{r},t), \quad (10)$$

where $\boldsymbol{\sigma}$ is the Pauli matrix and the magnetic field $\mathbf{B}(\eta) = \nabla \times \mathbf{A}(\eta)$. The solution to Eq. (10) is of the form

$$\phi_{\mathbf{p},\xi}(\mathbf{r},t) = \exp(-iE_{\mathbf{p}}t + i\mathbf{p}\cdot\mathbf{r})G_M(\eta)F_0(\eta)u_\xi, \quad (11)$$

TABLE II. Spin-channel-resolved scaled transition probabilities and the corresponding $\langle p_z \rangle$.

Channels	$\langle p_z \rangle$ (a.u.)	Scaled probability
Spin up → spin up	0.0072	1
Spin up → spin down	0.0075	6.8×10^{-6}
Spin down → spin up	0.0074	3.7×10^{-5}
Spin down → spin down	0.0072	1
Spin-0 approximation	0.0072	1

where $F_0(\eta) = \exp\left(\begin{smallmatrix} 0 & A_- \\ A_+ & 0 \end{smallmatrix}\right) f_0(\eta)$ with $A_\pm(\eta) = \mp [A_x(\eta) \pm iA_y(\eta)]/[2c(1 - p_z/c)]$ and u_ξ stands for the spinor basis $\binom{1}{0}$ and $\binom{0}{1}$. The matrix function is $G_M(\eta) = T(\exp\{i \int^\eta d\xi [F_0^\dagger(\xi)(d^2/d\xi^2)F_0(\xi)]/[2c^2(1 - p_z/c)]\})$. Following same procedures applied for spin-0 particles, one may obtain the transition amplitude containing the spin-magnetic coupling. The longitudinal momenta $\langle p_z \rangle$ associated with different spin evolution channels are summarized in Table II. The laser parameters are chosen to be of wavelength 1400 nm, intensity 10^{14} W/cm^2 and right-handed circularly polarized. The probability of spin flip is proportional to $I\omega^2$ with I being the intensity. For parameters used in this Letter and recent published experimental results [30], the probability of spin flip is significantly smaller than that of spin preservation. One may clearly see from Table II that the introduction of spin in the photoionization does not bring much difference for the longitudinal momentum shift.

In conclusion, the standard nondipole SFA theory, with or without rescattering, is built based on the exact nondipole Volkov wave function in nonrelativistic regimes. This theory can quantitatively reproduce the experimentally measured longitudinal momentum shift driven by linearly and circularly polarized laser pulses and disentangle the contributions of direct and rescattering ionization. Our work could be further extended to study processes such as high harmonic generations, nonsequential double ionization, and electron holography when nondipole effects are unavoidable. Thus, this work provides a solid foundation for research of laser-matter interactions, especially for the ultrafast processes triggered by strong midinfrared laser pulses which are popularly used now.

This work was supported by National Natural Science Foundation of China (Grants No. 11574205, No. 11322438, No. 11421064 and No. 11327902). Simulations were performed on the π supercomputer at 306 Shanghai Jiao Tong University.

*a225633@sjtu.edu.cn
†Present address: School of Physics, Georgia Institute of Technology, Atlanta, Georgia 30332, USA.
‡fhe@sjtu.edu.cn

[1] M. Uiberacker, Th. Uphues, M. Schultze, A. J. Verhoef, V. Yakovlev, M. F. Kling, J. Rauschenberger, N. M. Kabachnik, H. Schröder, M. Lezius, K. L. Kompa, H.-G. Muller, M. J. J. Vrakking, S. Hendel, U. Kleineberg, U. Heinzmann, M. Drescher, and F. Krausz, Attosecond real-time observation of electron tunnelling in atoms, Nature (London) **446**, 627 (2007).
[2] P. M. Paul, E. S. Toma, P. Breger, G. Mullot, F. Augé, Ph. Balcou, H. G. Muller, and P. Agostini, Observation of a train of attosecond pulses from high harmonic generation, Science **292**, 1689 (2001).
[3] W. Becker, X. Liu, P. Ho, and J. H. Eberly, Theories of photoelectron correlation in laser-driven multiple atomic ionization, Rev. Mod. Phys. **84**, 1011 (2012),
[4] V. Roudnev, B. D. Esry, and I. Ben-Itzhak, **HD**$^+$ and $\mathbf{H}_2^+$ Dissociation with the Carrier-Envelope Phase Difference of an Intense Ultrashort Laser Pulse, Phys. Rev. Lett. **93**, 163601 (2004).
[5] M. F. Kling, Ch. Siedschlag, A. J. Verhoef, J. I. Khan, M. Schultze, Th. Uphues, Y. Ni, M. Uiberacker, M. Drescher, F. Krausz, and M. J. J. Vrakking, Control of electron localization in molecular dissociation, Science **312**, 246 (2006).
[6] F. He, C. Ruiz, and A. Becker, Control of Electron Excitation and Localization in the Dissociation of $\mathbf{H}_2^+$ and its Isotopes Using Two Sequential Ultrashort Laser Pulses, Phys. Rev. Lett. **99**, 083002 (2007).
[7] G. Sansone, F. Kelkensberg, J. F. Pérez-Torres, F. Morales, M. F. Kling, W. Siu, O. Ghafur, P. Johnsson, M. Swoboda, E. Benedetti, F. Ferrari, F. Lépine, J. L. Sanz-Vicario, S. Zherebtsov, I. Znakovskaya, A. L'Huillier, M. Yu. Ivanov, M. Nisoli, F. Martín, and M. J. J. Vrakking, Electron localization following attosecond molecular photoionization, Nature (London) **465**, 763 (2010).
[8] W. B. Zhang, Z. C. Li, P. F. Lu, X. C. Gong, Q. Y. Song, Q. Y. Ji, K. Lin, J. Y Ma, F. He, H. P. Zeng, and J. Wu, Photon Energy Deposition in Strong-Field Single Ionization of Multielectron Molecules, Phys. Rev. Lett. **117**, 103002 (2016).
[9] C. T. L. Smeenk, L. Arissian, B. Zhou, A. Mysyrowicz, D. M. Villeneuve, A. Staudte, and P. B. Corkum, Partitioning of the Linear Photon Momentum in Multiphoton Ionization, Phys. Rev. Lett. **106**, 193002 (2011).
[10] A. Ludwig, J. Maurer, B. W. Mayer, C. R. Phillips, L. Gallmann, and U. Keller, Breakdown of the Dipole Approximation in Strong-Field Ionization, Phys. Rev. Lett. **113**, 243001 (2014).
[11] I. A. Ivanov, Relativistic calculation of the electronmomentum shift in tunneling ionization, Phys. Rev. A **91**, 043410 (2015).
[12] S. Chelkowski, A. D. Bandrauk, and P. B. Corkum, Photon-momentum transfer in multiphoton ionization and in time-resolved holography with photoelectrons, Phys. Rev. A **92**, 051401 (2015).
[13] I. A. Ivanov, J. Dubau, and K. T. Kim, Nondipole effects in strong-field ionization, Phys. Rev. A **94**, 033405 (2016).
[14] J. Liu, Q. Z. Xia, J. F. Tao, and L. B. Fu, Coulomb effects in photon-momentum partitioning during atomic ionization by intense linearly polarized light, Phys. Rev. A **87**, 041403 (2013).

[15] A. S. Titi and G. W. F. Drake, Quantum theory of longitudinal momentum transfer in above-threshold ionization, Phys. Rev. A **85**, 041404 (2012).
[16] H. R. Reiss, Relativistic effects in nonrelativistic ionization, Phys. Rev. A **87**, 033421 (2013).
[17] H. R. Reiss, Mass shell of strong field quantum electrodynamics, Phys. Rev. A **89**, 022116 (2014).
[18] D. Cricchio, E. Fiordilino, and K. Z. Hatsagortsyan, Momentum partition between constituents of exotic atoms during laser-induced tunneling ionization, Phys. Rev. A **92**, 023408 (2015).
[19] S. Chelkowski, A. D. Bandrauk, and P. B. Corkum, Photon Momentum Sharing between an Electron and an Ion in Photoionization: from One-Photon (Photoelectric Effect) to Multiphoton Absorption, Phys. Rev. Lett. **113**, 263005 (2014).
[20] D. Lao, P. L. He, and Feng He, Longitudinal photoelectron momentum shifts induced by absorbing a single XUV photon in diatomic molecules, Phys. Rev. A **93**, 063403 (2016).
[21] K. Krajewska and J. Z. Kamiński, Radiation pressure in strong field-approximation theory: Retardation and recoil corrections, Phys. Rev. A **92**, 043419 (2015).
[22] M. W. Walser, C. H. Keitel, A. Scrinzi, and T. Brabec, High Harmonic Generation beyond the Electric Dipole Approximation, Phys. Rev. Lett. **85**, 5082 (2000).
[23] N. J. Kylstra, R. M. Potvliege, and C. J. Joachain, Photon emission by ions interacting with short intense laser pulses: Beyond the dipole approximation, J. Phys. B **34**, L55 (2001).
[24] M. Verschl and C. H. Keitel, Analytical approach to wave packet dynamics of laser-driven particles beyond the dipole approximation, Laser Phys. **15**, 529 (2005).
[25] F. J. Dyson, The radiation theories of Tomonaga, Schwinger, and Feynman, Phys. Rev. **75**, 486 (1949).
[26] See Supplemental Material at http://link.aps.org/supplemental/10.1103/PhysRevLett.118.163203 for more details of the formula derivative and theory-experiment comparison, which includes Refs. [27,28].
[27] E. E. Serebryannikov and A. M. Zheltikov, Strong-Field Photoionization as Excited-State Tunneling, Phys. Rev. Lett. **116**, 123901 (2016).
[28] B. Hu, J. Liu, and S. G. Chen, Plateau in above-threshold-ionization spectra and chaotic behavior in rescattering processes, Phys. Lett. A **236**, 533 (1997).
[29] I. Barth and O. Smirnova, Spin-polarized electrons produced by strong-field ionization, Phys. Rev. A **87**, 065401 (2013).
[30] A. Hartung, F. Morales, M. Kunitski, K. Henrichs, A. Laucke, M. Richter, T. Jahnke, A. Kalinin, M. Schöffler, L. P. H. Schmidt, M. Ivanov, O. Smirnova, and R. Dörner, Electron spin polarization in strong-field ionization of xenon atoms, Nat. Photonics **10**, 526 (2016).
[31] V. S. Popov, Imaginary-time method in quantum mechanics and field theory, Phys. At. Nucl. **68**, 686 (2005).
[32] M. Klaiber, E. Yakaboylu, H. Bauke, K. Z. Hatsagortsyan, and C. H. Keitel, Under-the-Barrier Dynamics in Laser Induced Relativistic Tunneling, Phys. Rev. Lett. **110**, 153004 (2013).
[33] D. B. Milošević, Reexamination of the improved strong-field approximation: Low-energy structures in the above-threshold-ionization spectra for short-range potentials, Phys. Rev. A **88**, 023417 (2013).
[34] V. B. Berestetskii, E. M. Lifshitz, and L. P. Pitaevskii, *Quantum Electrodynamics*, 2nd ed. (Butterworth-Heinemann, Oxford, 1982).